

RESEARCH

Open Access



Optimized diagnosis of local anomalies in charge and discharge of solar cell capacitors

Xianhua Liu¹ and Qinghong Liu^{1*}

*Correspondence:
qhliu1003@126.com

¹ Information and Media
Institute, Jilin Province Economic
Management Cadre College,
Changchun 130000, China

Abstract

Background: With the increasingly serious environmental pollution and natural environment damage, renewable energy such as solar cells have gradually become the key to change this situation. Therefore, the local abnormal diagnosis of the charge and discharge of solar cell capacitors is particularly important.

Objective: To extend the life of ultracapacitors by resolving the issue of their low detection rate and enhancing the capacity to recognize fault diagnosis factors. A novel approach to charging and discharging, as well as the diagnosis of local anomalies, is put forth, utilizing switching networks.

Methods: By controlling the capacitors of multiple solar cells and supercapacitors to work together, it is possible to compensate for the shortage of photovoltaic power. The performance of fault diagnosis is optimized by combining principal component analysis and binary K-means clustering, which completes the fault diagnosis of capacitors.

Results: The experimental results show that the research method can increase the maximum output power of photovoltaic by 32.9% under multi-layer shadows. In the charging state of the training set, the number of abnormal capacitors is 6, and the number of normal capacitors is 12, and both of them are in accordance with the preset value. The number of abnormal capacitors and normal capacitors in the discharge state is the same as that in the charging state, which is also 6 and 12.

Conclusion: The research method can effectively address the issue of unbalanced energy storage battery packs and minimize the impact of local shadows on photovoltaic systems. In comparison to fuzzy C-means clustering, this method requires fewer iterations, enables faster fault diagnosis, and produces more accurate clustering results. It can provide technical support for diagnosing local abnormalities in the charging and discharging of solar cell capacitors.

Keywords: Batteries, Capacitor devices, Anomalies, Diagnostics, Dichotomous K-mean clustering algorithm

Introduction

Renewable energy has evolved into a necessity in people's social lives as a result of the environment's slow but steady decline (Nakhli et al. 2022). Solar energy is unrenowable, secure, and healthy as a kind of energy (Yassin et al. 2022). A photovoltaic battery, or Solar Battery (SB), is a device that transforms solar radiation energy directly into

electrical energy (Boldoo et al. 2022). A crucial component of the energy storage system, which is typified by immediate high power, is the Super Capacitor (SC) (Rezzak and Boudjerda 2020). Current research on ultracapacitor fault diagnosis focuses primarily on monitoring abnormal states. However, measuring the initial state during testing can increase costs. Therefore, it is important to provide a fault monitoring and analysis method during ultracapacitor monitoring to effectively process collected data and avoid data redundancy. Currently, the clustering method is commonly utilized in fault diagnosis, with a particular emphasis on fault identification of ultracapacitors (Falehi and Torkaman 2021). Principal Component Analysis (PCA) is a useful technique for reducing data dimensionality and highlighting abnormal data characteristics. By using PCA for dimensionality reduction, the bipartite K-means clustering algorithm can improve clustering efficiency and more effectively identify abnormal data or minority groups. Based on these problems, the study creates a novel PCA and Dichotomous K-mean clustering algorithm (DK-mCA) combination to detect abnormalities in Capacitor Device (CD) charging and discharging and to regulate CD charging and discharging. The study also confirms the efficiency of the suggested approach. The paper introduces two new concepts: The first method combines PCA and DK-mCA to reduce the training label data, improve anomaly detection efficiency, and reduce calculation costs. The second method uses a switching network to control capacitor charge and discharge, reducing the number of switching actions and minimizing the impact of photovoltaic power fluctuations on power system stability. The study is broken down into four sections: an overview of CD-related studies in SB is presented in the first section, the specific design of the Diagnosis of Local Anomalies in Charging and Discharging (DLACD) methodology is covered in the second section, the analysis of the DLACD methodology's findings is covered in the third section, and the study's conclusion is presented in the fourth section.

Related works

With the development of socio-economic and environmental concepts, the demand for SB's CD is increasing, and research related to SB's CD is also increasing. Karunanithi and others designed an independent photovoltaic system with a hybrid energy storage system. The system can release its energy under the condition of frequent load changes. Under constant load conditions, supercapacitors were responsible for providing the required energy to the load. The stability of the system was verified by experiments (Karunanithi et al. 2023). The performance of an integrated stand-alone hybrid power generating system at a site was evaluated by Salameh et al. and other experts in order to analyze the function of renewable energy resources. The hybrid energy system was modeled and simulated using specialized software. According to the experimental findings, the system can efficiently cut energy expenditures while reducing greenhouse gas emissions by roughly 83% (Salameh et al. 2021). Murthy et al. analyzed the impact of device structure on the performance of organic photovoltaic devices. They measured the charge transfer between the active layer and the bottom transport layer using surface photovoltage spectroscopy. The devices were studied experimentally and virtually. According to the experimental findings, conventional organic photovoltaic devices perform better in terms of device current density–voltage (Murthy et al. 2020). Rajulapati and Mahalingam presented a high gain

non-isolated multi-input dc–dc converter, which is driven by two distinct low voltage power supply, in order to integrate the low voltage photovoltaic inputs to the common DC bus. According to the experimental findings, the high gain concept and the equalization technique put forward in the study were both fully practical (Rajulapati and Mahalingam 2022). To examine the impact of nanocomposite repair on capacitive electrodes, Ingrosso et al. chemically created a new hybrid nanocomposite material. The study's findings demonstrated that the substance has a greater electrochemical specific capacitance, and its restored electrodes would function as an electrochemical SC device (Ingrosso et al. 2021).

In order to evaluate the performance of the converter that should be utilized for commercial fuel cells and photovoltaics, Dhimish and Schofield illustrated how a single switch unidirectional step-up and down dc–dc converter operates. This dc–dc converter can be operated over a wide input voltage range. The experimental results indicated that the converter obtains efficiency ranges up to 90% and achieves efficiencies above 90% (Dhimish and Schofield 2022). To analyze the regenerative system of a hybrid tram for propulsion of a tram track, Paul Arévalo et al. carried out a modeling and control study of the system and analyzed the different renewable hybrid systems. In addition, the composition of the system was mainly made up of renewable energy sources. According to the experimental findings, the system can both effectively cut greenhouse gas emissions and energy costs (Arévalo et al. 2021). Sarker et al. used SB capacitance simulator to develop a new tandem solar device and verified the structure of the single junction device they constructed. The findings of the experiment indicated that the simulated outcomes are accurate and have good resilience (Sarker et al. 2021). Alzoubi et al. developed a new method to enhance the efficiency of SB by using silicon. This method improves the photovoltaic performance parameters of the SB device. The experimental results showed that the method maintains good stability even at high temperatures and significantly improves the quantum efficiency (Alzoubi et al. 2021). Ren et al. proposed a novel two-step annealing process in order to obtain high-quality copper-zinc-tin-selenide-sulfide absorbers. The experimental results demonstrated that the average efficiency of the device was improved by 6% overall. In addition, the process can inhibit the decomposition of copper-zinc-tin-selenide sulfides during the annealing process (Ren et al. 2020).

In summary, local shadows can often appear in photovoltaic arrays due to obstructions from buildings, trees, and other structures. These shadows can cause uneven lighting and differences in module output characteristics, which can negatively impact the efficiency of photovoltaic power generation. Currently, the K-means clustering method is the most commonly used approach for fault identification. However, it may produce errors due to its dependence on the initial clustering center. The binary K-means clustering algorithm has been improved for fault diagnosis of supercapacitor modules. To address these issues, a solar cell supercapacitor based on a switching network is proposed, and the PCA method and binary K-means clustering algorithm are combined. The proposed method can effectively address the issue of unbalanced energy storage in battery packs, indirectly enhancing the accuracy of the maximum power tracking algorithm, reducing the number of switching actions, and improving fault detection efficiency.

CDDLACD method design for SB

In order to design the CDDLACD method for SB, the study has designed the control method for CD charging and discharging on the basis of switching network. In addition, the study constructs the CD charging/discharging anomaly diagnosis method by PCA and DK-mCA.

Design of CD charging and discharging control method based on switching networks

Solar Cell-supercapacitor Device (SCSD) has a combined function of power generation and energy storage, so in order to have a solution for the multi-peak problem of PV output power, the study designs a grid-connected PV architecture based on SCSD. In order to verify the functionality of this CD, the study analyses the operating characteristics of the SCSD. The equivalent circuit and the specific architecture of the SCSD are shown in Fig. 1.

In Fig. 1, the architecture of the SCSD is divided into two units in its entirety, the SB unit and the SC unit. In addition, the specific architecture of SCSD involves different ports, positive electrodes, back electrodes, capacitive anodes, electrolytes, counter electrodes and silicon P–N Junction (PN) nodes. The solar cell unit consists of a positive electrode, a silicon PN section, a back electrode, and a capacitive anode. The ultracapacitor unit consists of a back electrode, a capacitive anode, an electrolyte, and a counterelectrode. A mathematical model can show the output current of numerous series-connected photovoltaic cells under uniform illumination from the sun. The specific engineering mathematical model is shown in Eq. (1).

$$\begin{cases} C_1 = \left(1 - \frac{I_m}{I_{SC}}\right) \exp\left(-\frac{V_m}{C_2 V_{oc}}\right) \\ I = I_{SC} \left\{1 - C_1 \left[-1 + \exp\left(\frac{V/n}{C_2 V_{oc}}\right)\right]\right\} \\ C_2 = \left(\frac{V_m}{V_{oc}} - 1\right) \left[\ln\left(1 - \frac{I_m}{I_{SC}}\right)\right]^{-1} \end{cases} \quad (1)$$

In Eq. (1), V represents the PV cell output voltage. It is the voltage at both ends of the output end of the photovoltaic cell under certain specific conditions such as light or temperature. V_{oc} denotes the PV cell open-circuit voltage. It refers to the voltage when the output end of the battery is completely open. V_m denotes the maximum power point

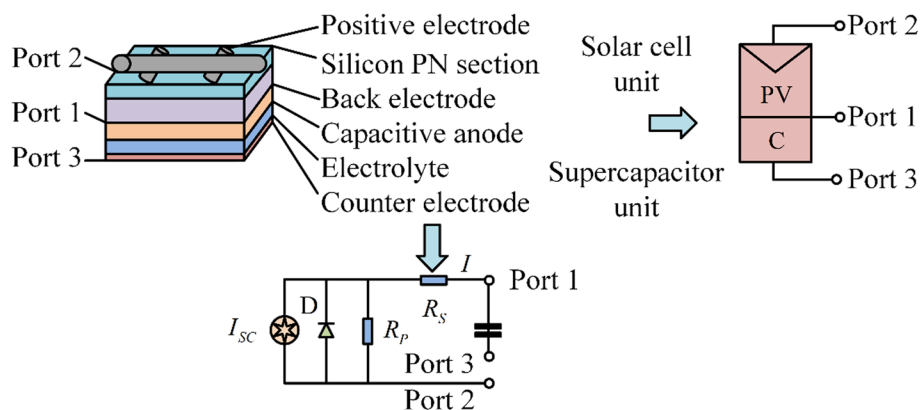


Fig. 1 Equivalent circuit and specific architecture of SCSD

voltage. It is the voltage corresponding to the maximum power output of the photovoltaic cell under specific conditions. I is the PV cell output current. The current generated by the battery is dependent on various conditions, such as light intensity and battery temperature. I_{SC} denotes the PV cell short-circuit current. It refers to the current flowing through the battery when the two ends of the battery are directly shorted, representing the maximum current that the battery can produce under a given light condition. I_m denotes the maximum power point current. This refers to the current when the photovoltaic cell reaches the maximum power point. C_1 and C_2 are both the introductory quantities. It refers to the impact of some additional factors in the photovoltaic system, such as temperature and light, on the performance of the battery. and n denotes the number of series-connected PV cells. The number of individual cells that are connected together in series in a photovoltaic panel or system. When the solar illumination conditions of all n SCSDs are standard, the expressions of output current and power of the series branch are shown in Eq. (2) (Maihulla et al. 2022).

$$\begin{cases} I = I_{SC} \left\{ 1 - C_1 \left[\exp \left(\frac{V/n}{C_2 V_{oc}} \right) - 1 \right] \right\} \\ P = \sum_{j=1}^n P_j = \sum_{j=1}^n I_j V_j \end{cases} \quad (2)$$

In Eq. (2), P is the output power of the series branch, j represents the serial number of the SCSD, I_j represents the output current of the j th SCSD, P_j is the output power of the j th SCSD, and V_j represents the output voltage of the j th SCSD. When a SCSD is shaded and the degree of shading is mild, the total output current of that shaded SCSD is shown in Eq. (3).

$$I_{i,S} + I_{ci} = I_j = I \quad (j = 1, \dots, n, j \neq i). \quad (3)$$

In Eq. (3), i is the serial number of the shaded SCSD and it is not equal to the serial number of the SCSD, j . $I_{i,S}$ represents the output current of the i th shaded SCSD PV cell, and I_{ci} represents the output current of the i th shaded SCSDSC. When the shadow masking disappears, the output current and power of the series branch are shown in Eq. (4).

$$\begin{cases} I = I_{SCi,S} \left\{ 1 - C_1 \left[\exp \left(\frac{V/n}{C_2 V_{oc}} \right) - 1 \right] \right\} + I_{ci} = I_{SC} \left\{ 1 - C_1 \left[\exp \left(\frac{V/n}{C_2 V_{oc}} \right) - 1 \right] \right\} \\ P = P_1 + \dots + (P_{i,S} + P_{ci}) + \dots + P_n = \sum_{j=1}^n P_j \end{cases} \quad (4)$$

In Eq. (4), $I_{SCi,S}$ represents the short-circuit current of the PV cell under the shadow, $P_{i,S}$ represents the PV cell output power of the i th SCSD under the shadow, P_n is the PV cell output power of the n th SCSD, and P_{ci} represents the SC output power of the i th SCSD under the shadow. When the SCSDs are heavily shaded, the total output current of the i th SCSD cannot reach the PV output current of the other SCSDs, as shown in Eq. (5).

$$I_{i,S} + I_{ci} < I_j = I \quad (j = 1, \dots, n, j \neq i). \quad (5)$$

When conditions such as array structure and light intensity are determined, the load impedance then determines the position of the PV array in the characteristic curve. When the load impedance is less, the output current and output power of SCSD are shown in Eq. (6).

$$\begin{cases} I = I_{SC} \left\{ 1 - C_1 \left[\exp \left(\frac{V/n-1}{C_2 V_{oc}} \right) - 1 \right] \right\} \\ P = \sum_{j=1}^n P_j - P_i \end{cases} \quad I_{i,S} + I_{ci} < I \leq I_j. \tag{6}$$

In Eq. (6), P_i represents the PV cell output power of the i th SCSD. When the load impedance increases, the value of I decreases gradually, and the output current and power of the series branch at this time are expressed as shown in Eq. (7).

$$\begin{cases} I = I_{SCi,S} \left\{ 1 - C_1 \left[\exp \left(\frac{V/n}{C_2 V_{oc}} \right) - 1 \right] \right\} + I_{ci} \\ P = n(P_{i,S} + P_{ci}) \end{cases} \quad 0 \leq I < I_{i,S} + I_{ci}. \tag{7}$$

In Eq. (7), $I_{SCi,S}$ represents the short-circuit current of the PV cell in the shaded i th SCSD. $n \times m$ series-parallel PV array has a basic structure of SCDCs and it employs an inverter and a transformer for grid connection. By controlling switch B, each SCDC in the PV array can employ SB to charge the SCs. The specific architecture of the SCDC based PV system is shown in Fig. 2.

The SCDC-based PV power system design is depicted in Fig. 2, and each SCDC unit has three ports of its own. In addition, the system also involves switching network, grid, transformer, inverter and maximum power tracking template. $n \times m$ series-parallel PV array as a whole has $mn \cdot mn$ switches, where the main diagonal switching Boost converter can compensate its own power, while the non-main diagonal

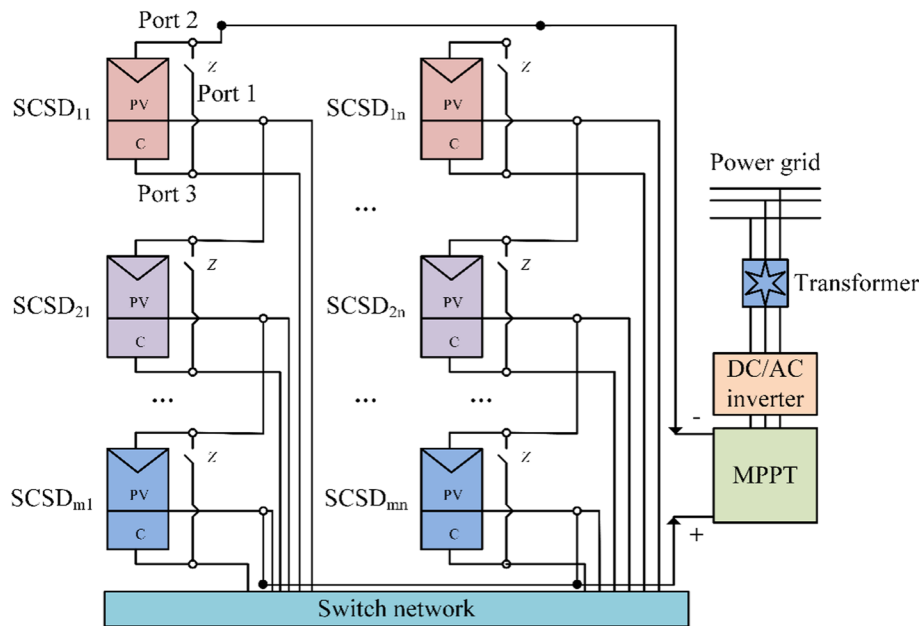


Fig. 2 Specific architecture of SCDC based photovoltaic power generation system

switching Boost converter compensates the power of other SCDC units. Controlling the changes in the state of the Boost converters in the switching network can be a solution to the problem of underpowered SCDCs themselves in heavy and multi-layered shadows. In order to make a simplification of the complexity of the charging control, the study sets the principle of SC charging, i.e., the SC is charged only when the sunlight is sufficient. The calculation of light intensity is shown in Eq. (8).

$$G = \frac{P_G}{\eta S [1 + 0.005(t_o + 25)]}. \quad (8)$$

In Eq. (8), G represents the light intensity, η represents the conversion efficiency, S represents the area of the PV panel, t_o is the temperature, and P_G represents the output power of the lower PV array. When the PV array is set up, both η and S are known parameters and when the effect of temperature is not considered, the expression of the switching control principle is shown in Eq. (9).

$$Z = \begin{cases} 1 & G > 1000 \\ 0 & G \leq 1000 \end{cases}. \quad (9)$$

In Eq. (9), Z denotes the switch, 1 represents for the closed state, and 0 represents for the disconnected state. The SC discharge is mainly realized by on-off control of the switching tubes of the Boost converter, and the expression of its own state-space equations after removing the factors such as the internal resistance loss of the Boost converter is shown in Eq. (10).

$$\begin{cases} L \frac{di_L}{dt} = u_C - (1 - D)u_o \\ C_P \frac{du_o}{dt} = (1 - D)i_L - \frac{u_o}{R} \end{cases}. \quad (10)$$

In Eq. (10), L is the series inductance value. In a DC-DC converter, an inductor is used to store and release energy, and its ability to store energy is proportional to its inductance value. R is the load resistance. The load resistance is a measure of the degree to which the load obstructs the current of the circuit, and its change causes the output voltage and current to change. The duty cycle D of the switching tube varies at different moments and is determined based on the design requirements and load characteristics of the power supply. In practical applications, the optimal duty cycle is typically found through theoretical calculation and experimental adjustment. The duty cycle of the switching tube directly affects the output voltage, current and power conversion efficiency of the power supply. i_L represents the average value of the inductor current during the switching cycle. The magnitude and range of inductance current affect the energy transfer efficiency and output ripple. u_o represents the average value of the capacitor voltage during the switching cycle. The magnitude and range of inductance current affect the energy transfer efficiency and output ripple. u_C denotes the voltage at the SC terminal. It refers to the voltage corresponding to the electrical energy stored in the ultracapacitor, which is usually used to provide an instantaneous high current or as an energy storage element. C_P represents the value of the shunt capacitance. It is usually used in the output of the power supply or other

parts of the circuit to improve the stability of the power supply and reduce the output ripple.

Construction of CD charge–discharge abnormal diagnosis method based on principal component analysis and DK-mC

As an energy storage device between capacitors and batteries, SCs are not only capable of fast charging and discharging, but also of energy storage (Ying et al. 2022). SCs can be divided into three kinds from the whole, and one of them, the double electric layer capacitor, not only has excellent reversibility, but also features high charging and discharging efficiencies and high power densities (Sajjad et al. 2021). The specific composition structure of double electric layer capacitor is shown in Fig. 3.

In Fig. 3, the structure of a double layer capacitor can be divided into three parts on the whole, which are diaphragm, electrolyte and electrode. Among them, the electrode part involves four aspects, which are electrode material, conductive agent, binder and collector. The diaphragm part mainly includes non-woven diaphragm and cellulose diaphragm. The electrolyte part involves three aspects, which are inorganic electrolyte, organic electrolyte and ionic electrolyte. When the SC runs at high intensity for a long time, various substances produced inside it will block its own air holes, and this can easily lead to the phenomenon of electrode cracking (Verkholyak et al. 2022; Uno et al. 2023). In addition, there are also many influencing factors that can accelerate the aging of SC apparatus, and the specific influencing factors are shown in Fig. 4.

As shown in Fig. 4, the influencing factors of SC apparatus aging can be mainly divided into internal and external influencing factors, of which the internal influencing factors are mainly the self-accelerating aging of the capacitor itself. The external influencing factors can be mainly divided into five parts, which are the user's need to use, the characteristics of the product itself, temperature, voltage and current. Among them, the temperature includes the initial stable temperature rise and the working temperature. User needs involve three aspects, namely, current waveform, voltage level and operating temperature. Voltage includes two aspects, bias voltage and depth of discharge. The current part includes three aspects, which are charging and discharging times, current change rate and root mean square current. The characteristics of the product itself involves three aspects of rated current multiplier, rated voltage range and rated operating temperature. The common anomaly detection methods for SCs are mathematical

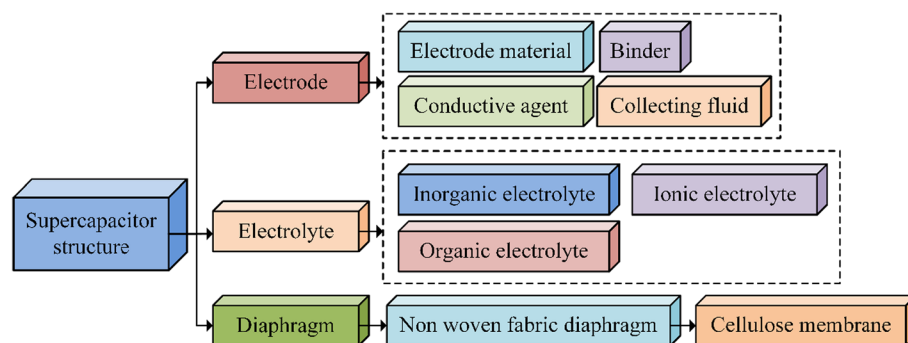


Fig. 3 Specific composition and structure of Supercapacitor

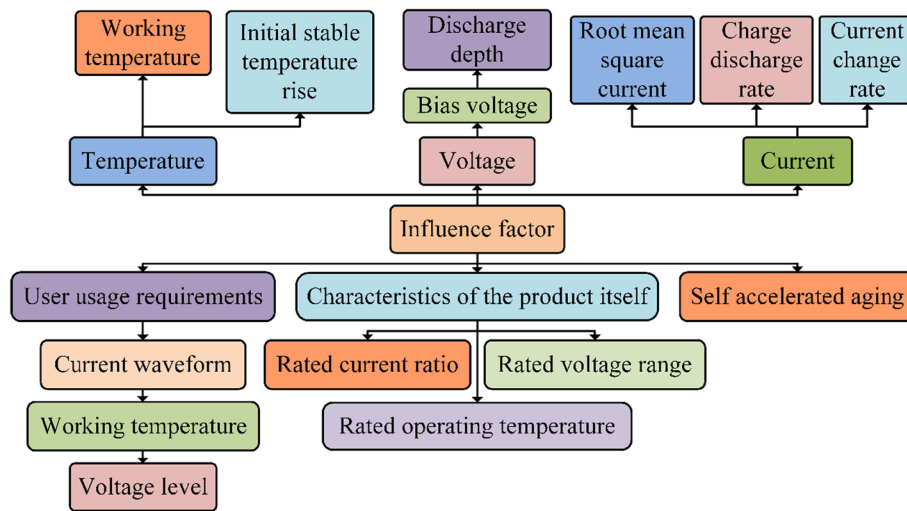


Fig. 4 Factors affecting the aging of supercapacitors

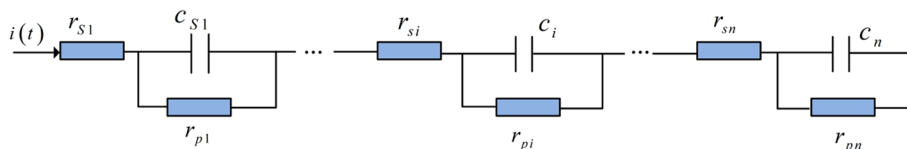


Fig. 5 Equivalent circuit diagram of series supercapacitor bank

modeling and online identification of parameters. PCA is an effective method for reducing data dimensionality and highlighting anomalous data characteristics. The binary K-means clustering algorithm can improve clustering efficiency through PCA dimensionality reduction. Compared to other technologies, binary K-means clustering performs better in processing large datasets and identifying non-spherical clusters. The paper suggests an anomaly detection approach based on Dichotomous K-mean clustering (DK-mC) and PCA in order to lessen the difficulty and expense of the detection. The series SC group equivalent circuit is shown in Fig. 5.

As shown in Fig. 5, when the SC is running, its own charging and discharging currents are the same. The voltage profile can demonstrate the data obtained in the sensor, but not the variation of the internal parameters of the SC, so the selected characteristic quantity needs to represent the state of the SC itself. The relationship between the difference between the SC terminal voltage measurements near the time and the SC current is shown in Eq. (11).

$$C_i \times [-u_{Ci}(t - \Delta t) + u_{Ci}(t)] = [i(t - \Delta t) + i(t)] \times \frac{\Delta t}{2}. \tag{11}$$

In Eq. (11), t is the moment, $u_{Ci}(t)$ represents the SC voltage at t , $i(t)$ represents the SC current at t , Δt is the sampling interval, C_i is the capacitance value of and the relationship equation removes the effect of leakage current. The relationship between the SC terminal voltage measurements at two adjacent moments is shown in Eq. (12).

$$u_i(t) - u_i(-\Delta t + t) = u_{Ci}(t) - u_{Ci}(-\Delta t + t) + r_{si} \times [-i(-\Delta t + t) + i(t)]. \quad (12)$$

In Eq. (12), $u_i(t)$ is the measured value of the SC terminal voltage at t , and r_{si} is the SC series resistance. The state matrix of the difference between the measured values of the terminal voltages of multiple series-connected monoblocks is shown in Eq. (13).

$$A_{n \times m} = \begin{bmatrix} \Delta u_{1,1} & \Delta u_{1,2} & \dots & \Delta u_{1,m} \\ \Delta u_{2,1} & \Delta u_{2,2} & \dots & \Delta u_{2,m} \\ \dots & \dots & \dots & \dots \\ \Delta u_{n,1} & \Delta u_{n,2} & \dots & \Delta u_{n,m} \end{bmatrix}. \quad (13)$$

In Eq. (13), Δu is the difference of the end voltage measurements. PCA can extract the eigenvalues of matrix $A_{n \times m}$ to improve the efficiency of anomaly diagnosis. PCA analysis is usually divided into five steps, of which the first step is the data preprocessing. The second and third steps are the judgement of the number of principal components to be selected, followed by the selection. The fourth step is the elaboration and interpretation of the results and the fifth step is the calculation of the scores of the principal components. The dichotomous K-means algorithm will have two clustering centers and divides the sample as a whole into two parts. In addition, the algorithm performs the next division by Sum of Squares for Error (SSE) and the smaller its value is the better the result. The calculation of SSE is shown in Eq. (14).

$$SSE = \sum_{\varepsilon=1}^k \sum_{x \in Q_\varepsilon} dist(q_\varepsilon, x)^2. \quad (14)$$

In Eq. (14), Q_ε represents the ε th category, $dist$ represents the Euclidean distance between samples, x is the samples in the sample set, k is the number of categories classified, and q_ε is the centre of mass of the ε th category Q_ε . The Euclidean distance between clusters is shown in Eq. (15).

$$dist(x_\varepsilon, x_\phi) = \left(\sum_{l=1}^n |x_\varepsilon^l - x_\phi^l|^2 \right)^{\frac{1}{2}}. \quad (15)$$

In Eq. (15), x^l is the l th eigenvalue, x_ϕ is the ϕ th sample in the sample set, and x_ε is the ε th sample in the sample set. The method flow of anomaly diagnosis is shown in Fig. 6.

The sampling calculation is the first stage in anomaly identification, as illustrated in Fig. 6, and the feature vector extraction from the clustered samples by PAC is the second. In the third phase, the variance of the feature vectors is calculated. If the criteria are satisfied, DK-mC is applied to the training samples, and the clustering centre is identified. The categories are classified in the fourth phase based on the computed distance between the test sample and the clustering centre. The fifth step is to reconstruct the new diagnostic model and finally end the process. The PCA parameter selection process involves choosing the number of principal components based on the cumulative variance contribution rate. This means that the first n principal components are selected to reach a predetermined threshold, in order to reduce noise and eliminate redundant information. For binary K-means clustering, the initial cluster center uses the K-means++ heuristic method to reduce initial selection bias and improve clustering efficiency and accuracy.

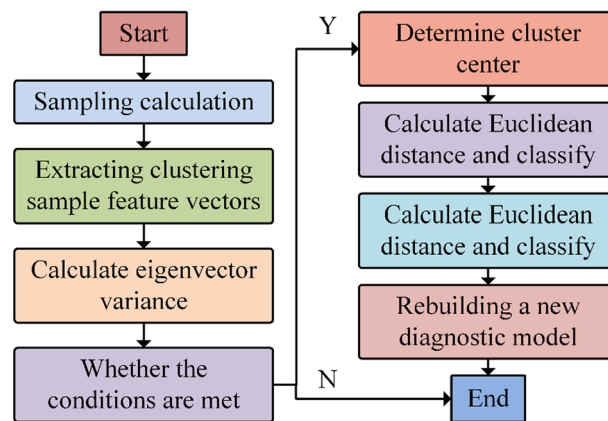


Fig. 6 Method and process of abnormal diagnosis

Table 1 Parameters of solar cells and ultracapacitors

Solar cell parameters				Supercapacitor parameter	
Solar cell parameters	Numerical value	Solar cell parameters	Numerical value	Supercapacitor parameter	Numerical value
Irradiance (W/m ²)	1000	Open circuit voltage (V)	36	Capacity	15
Power (W)	260	Maximum power point current (A)	9.02	Rated voltage (V)	48
Short circuit current (A)	9.71	Maximum power point voltage (V)	30	SOC range	10–90%

It is important to note that PCA reduces dimensionality based on linear transformation principles. However, for nonlinear data sets, this method may not effectively identify and retain important features. On the other hand, binary K-means clustering is more sensitive to the selection of publishing cluster center. The loss of abnormal data features or improper selection during dimensionality reduction can affect the accuracy of detection.

Analysis of CDDLACD results for SB

By examining the PV array’s output characteristics under various levels of shade, the study examines the viability of its suggested approach. In addition, the study has also set up various parameters for different degrees of shading conditions. In order to analyze the anomalous diagnostic results of SC charging and discharging, the study has selected several SC monoliths of rated voltage to perform series simulation experiments.

Analysis of results of CD charging and discharging control methods based on switching networks

The research object is a 4 × 3 series–parallel photovoltaic array composed of 12 SCSD modules. The initial conditions assume that the photovoltaic array is not shaded and the temperature is constant at 25 °C, and the parameters of the solar cell ultracapacitor module are shown in Table 1.

The output characteristics of both PV arrays are examined under various degrees of shadowing situations in order to compare the suggested approach of the study to the standard reconstruction method for comparison. For the shading conditions under different degrees, the study has set the shading masking for the data in the PV arrays with the intensity of sunlight. In addition, the light intensity of other SCDC units is also set. Figure 7 displays the adjusted PV array's output power curves for various levels of shade.

As demonstrated in Fig. 7a, the output power curve of the PV array before adjustment has two maximum values, 2.39 kW and 2.15 kW, when the degree of shadowing is light. the PV array has only one maximum value after compensation through the traditional method, with the value of 2.75 kW. The PV array also has only one maximum value after compensation through the proposed method of the study, with the value of 3.01 kW. According to Fig. 7b, the output power curve of the PV array before adjustment likewise has two maximum values, which are 1.91 kW and 1.22 kW, when the degree of shadowing is high. The PV array has only one maximum value after compensation through the conventional method, which has a value of 2.39 kW. The PV array also has only one maximum value after compensation by studying the proposed method, which is 2.93 kW. In Fig. 7c, when the shading condition is multi-layer shading, the output power curve of the PV array before compensation has three maxima, which are 1.88 kW, 1.77 kW and 1.52 kW, respectively. The PV array also has three maxima after compensation by the traditional method, which are 2.08 kW, 1.53 kW and 0.89 kW, respectively. The PV array compensated by the proposed method has only two maxima, 2.82 kW and 1.51 kW respectively, which shows that the PV array compensated by the proposed method has higher output power and can avoid the occurrence of multiple maxima to a certain extent. The research method can reduce the number of multiple peaks under multi-layer shadows, and the maximum output power of photovoltaic is increased by 32.9%. The comparison of SC homogenized waveforms for different capacitance values and initial voltages is shown in Fig. 8.

According to Fig. 8a, the maximum and minimum voltages of SC monomer 1 are 2.51 V and 2.01 V, respectively, when the capacitance values are the same but the starting voltages differ. The voltage of SC monomer 2 ranges from 0.97 V to 2.3 V at its greatest value. The voltage of SC monomer 3 can reach a high of 2.01 V and a minimum of 0.65 V. The voltage of SC monomer 4 can reach a high of 1.5 V and a minimum of 0 V. According to Fig. 8b, all four SC monomers have the same voltage maximum and minimum values, which are 2.82 V and 0 V, respectively, when the capacitance values are

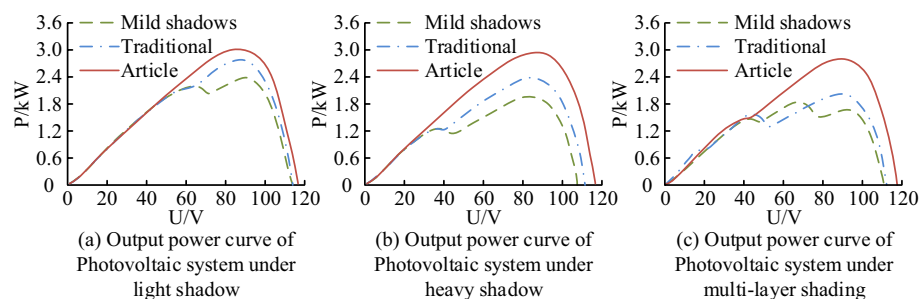


Fig. 7 A corrected photovoltaic system's output power curve under various shading scenarios

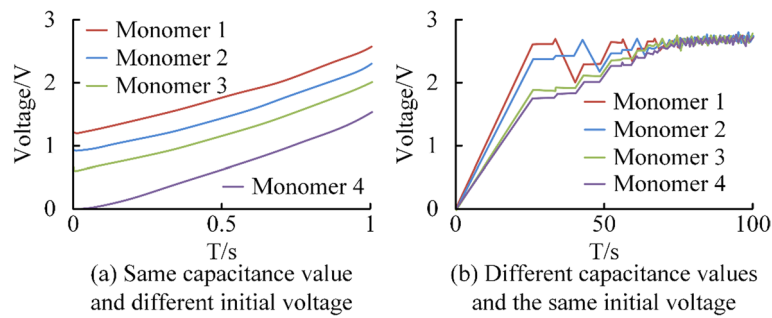


Fig. 8 Comparison of voltage sharing waveforms of supercapacitors under different capacitance values and initial voltage conditions

variable but the beginning voltages are the same. The maximum and minimum voltages of the four SC monomers, 2.82 V and 0 V, are the same when the capacitance values are different but the beginning voltages are the same, as can be shown in Fig. 8b. The voltage value of SC monomer 1 is higher than the other monomers at the same moment in time until the voltage value is close to the maximum value. In summary, the charging and discharging control method based on a switching network has a higher output power under local shadow and can realize independent charging and discharging control of single devices. This method can effectively avoid the unbalanced problem of the energy storage battery pack. Compared to traditional methods, the proposed SCSD-based photovoltaic array can effectively address the issue of multi-peak output power of photovoltaic arrays under local shadows. This improves the accuracy of the maximum power tracking algorithm and enhances the stability of power system operation.

CD charge–discharge abnormal diagnosis results based on PAC and DK-mC

A number of SC monomers with rated voltages are chosen for the investigation so that series simulation tests could be carried out to investigate the charging and discharging circumstances of SCs. In addition, the study divides the selected SC monoblocks into training samples and test samples. Among them, the training samples account for 75% and the test samples account for 25%. When setting the capacitance simulation parameters, the experiment uses the capacitance field's provided parameters as reference values. These include the capacitance value, series resistance, and parallel resistance value, which are 3500 F, 0.1 Ω , and 27 k Ω , respectively. It is important to note that the parameter settings for each capacitor are different. The experiment conducted a series simulation test on a 24 rated voltage and 2.7 V supercapacitor monomer. For this process, 18 ultracapacitor samples are selected as test samples. Two clustering centers are determined, and then 6 samples are selected for further testing. The simulation test is carried out under two conditions: charging and discharging. Table 2 displays the parameters of the SC monoblock training samples.

As shown in Table 2, the parameters of the SC monolithic training samples contain serial number, capacitance, series resistance and parallel resistance. The fuzzy C-mean clustering approach is chosen for the study to compare and discover abnormalities in charging and discharging conditions using these two methods and to better validate the performance of DK-mCA. The comparison of the charging and

Table 2 Sample parameters for supercapacitor unit training

Number	Capacitance (F)	Series resistor (Ω)	Parallel resistor (k Ω)	Number	Capacitance (F)	Series resistor (Ω)	Parallel resistor (k Ω)
1	2605	0.21	27.0013	10	3471	0.33	26.9362
2	3500	0.13	26.9423	11	3455	0.12	26.9586
3	2755	0.18	27.0384	12	2535	0.10	27.3503
4	3485	0.09	26.9886	13	3445	0.07	26.9703
5	2655	0.29	26.9862	14	2405	0.17	27.2303
6	3515	0.14	26.9819	15	3535	0.19	27.3403
7	3465	0.11	27.0811	16	3495	0.16	27.0501
8	3525	0.06	27.0467	17	3545	0.19	27.1006
9	3475	0.08	27.0416	18	3385	0.15	27.0603

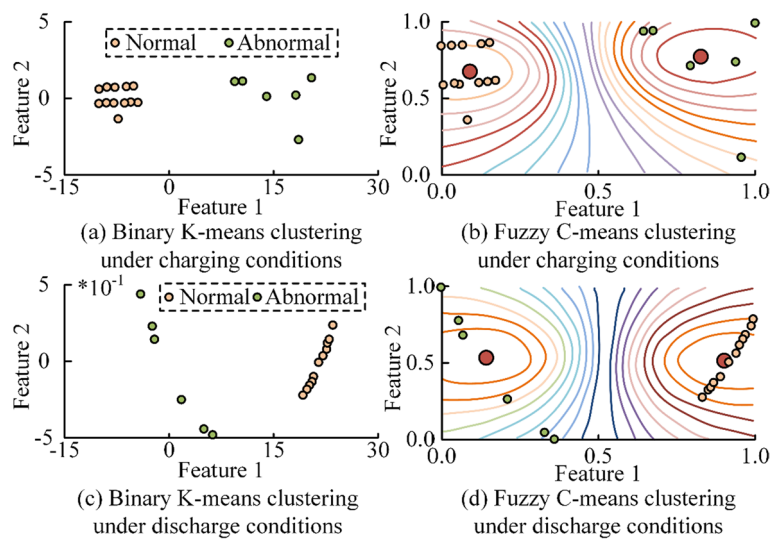


Fig. 9 Comparison of charging and discharging anomaly detection results of different algorithms on training samples

discharging anomaly detection results of DK-mCA and fuzzy C-mean clustering algorithm on the training samples is shown in Fig. 9.

In Fig. 9a, the orange circle in the charging state and DK-mCA stands in for the typical capacitance, which has a number of 12. The green circle represents the abnormal capacitance and its number is 6. The numbers of both abnormal and normal capacitors are in accordance with the preset values. As observed in Fig. 9b, the aberrant and normal capacitances discovered by the fuzzy C-mean clustering algorithm under the charging condition are consistent with those detected by DK-mCA and meet the predetermined values. The clustering’s focal point is the red circle. According to Fig. 9c, there are 6 abnormal capacitances and 12 normal capacitances under the discharged state and DK-mCA, both of which are commensurate with the predetermined values. According to Fig. 9d, the abnormal capacitance and normal capacitance are the same under the discharge condition and fuzzy C-mean clustering algorithm and adhere to

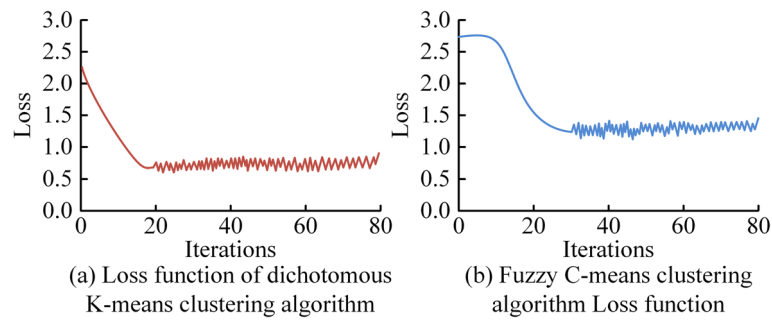


Fig. 10 Comparison of loss function between two algorithms

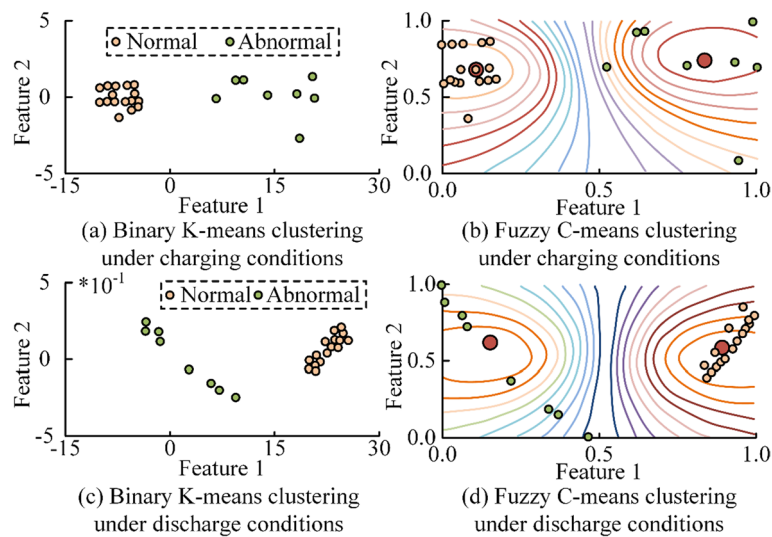


Fig. 11 Comparison of charging and discharging anomaly detection results between two algorithms after introducing test samples

the predetermined values. Comparison of the loss functions of the two algorithms is shown in Fig. 10.

The loss function of the DK-mCA has a maximum value of 2.3 and a minimum value of 0.7, as shown in Fig. 10a, and the trend tends to level off after 20 iterations. The fuzzy C-mean clustering algorithm's loss function has a maximum value of 2.7 and a minimum value of 1.3, as shown in Fig. 10b, and the trend tends to level off after 30 iterations. This shows that DK-mCA performs better. A comparison of the charging and discharging anomaly detection results of DK-mCA and fuzzy C-mean clustering algorithm after introducing test samples is shown in Fig. 11.

Figure 11a shows that under the charging state and DK-mCA, there are 16 normal capacitances and 8 aberrant capacitances, both of which are consistent with the preset values. The number of normal capacitance and abnormal capacitance under charging state and fuzzy C-mean clustering algorithm is consistent with that under DK-mCA, according to Fig. 11b. According to Fig. 11c, under the discharging state and DK-mCA, there are 16 normal capacitances and 8 aberrant capacitances, both of which are commensurate with the predetermined values. As demonstrated in Fig. 11d, the abnormal

capacitance and normal capacitance under the discharge state and fuzzy C-mean clustering technique are consistent with those under DK-mCA and meet the predetermined values. To compare the diagnostic accuracy, speed, computational efficiency, and error rate of the research method with existing methods, the SPSS 26.0 software is used to statistically analyze the data. For quantized data that follow a normal distribution, the mean \pm standard deviation is used. Categorical variables are compared using the Chi-square test (χ^2 test). The results are presented in Table 3.

Table 3 shows statistically significant differences ($P < 0.05$) between the proposed research method and the methods mentioned in literatures (Karunanithi et al. 2023; Sarker et al. 2021), and (Ren et al. 2020) in terms of diagnostic accuracy, computational efficiency, and prediction error rate. The proposed method outperforms the other three methods with a diagnostic accuracy of 93.3%. Additionally, the prediction error rate of the proposed method is 0.309, which is lower than the other three methods. However, this research method's computational efficiency is lower than that of the methods in references (Karunanithi et al. 2023) and (Sarker et al. 2021). The scheme needs to optimize the number of PCA components, which increases the number of iterations. As a result, the distance from data points to cluster centers and allocation steps can be calculated in parallel to optimize time.

Conclusion

The study ingeniously integrated PCA and DK-mCA to diagnose the local anomalies of CD charging and discharging of SB, and created the control mechanism based on CD charging and discharging of switching network. The testing results showed that even after adjusting by the method proposed by the study, the PV array only had one maximum value, with a value of 3.01 kW, when the degree of shade was mild. The PV array likewise only had one maximum value after correction by researching the suggested approach, with a value of 2.93 kW, when the degree of shade is severe. After adjustment by researching the suggested approach, the PV array only had two maximum values, with values of 2.82 kW and 1.51 kW, respectively, when the shading situation was multi-layer shading. There were 6 aberrant capacitors in the charging state and 12 normal capacitors in the training set, and both of these quantities were consistent with the preset values. In the discharged condition, there were the same number of aberrant and normal capacitors (6 and 12) as there were in the charged state. It was clear that the study's suggested technique performs well for diagnosing local anomalies of CD charge and discharge in SB. Although PCA and binary K-means clustering algorithms are theoretically capable

Table 3 Comparison results of fault monitoring performance of each method

Algorithm	Diagnostic accuracy rate, %	Calculate time efficiency, ms	Prediction error rate, %
References (Karunanithi et al. 2023)	0.781	89	0.342
References (Sarker et al. 2021)	0.802	85	0.369
References (Ren et al. 2020)	0.864	108	0.386
Research method	0.933	102	0.309
<i>P</i>	< 0.05	< 0.05	< 0.05

of handling high-dimensional data and identifying anomalous patterns, they need to be adapted to specific application scenarios. This research method has a wide range of practical applications, such as in building energy management systems used for monitoring and diagnosing the performance of solar panels and energy storage devices. The smart grid enables efficient management of distributed photovoltaic power generation resources and energy storage units. Further research will focus on developing a more intelligent energy management system for the integration and modular design of supercapacitors. This system will monitor photovoltaic output and supercapacitor status in real-time.

Author contributions

X.L. contributed to conceptualization, data curation, formal analysis, investigation, writing—original draft and Q.L. contributed to the methodology, visualization, writing—original draft, writing—review and editing.

Funding

Not applicable.

Availability of data and materials

The datasets generated during and/or analysed during the current study are available from the corresponding author on reasonable request.

Declarations

Ethics approval and consent to participate

Not applicable.

Consent for publication

Not applicable.

Competing interests

The authors declare no potential competing interests.

Received: 19 February 2024 Accepted: 10 April 2024

Published online: 20 April 2024

References

- Alzoubi T, Moghrabi A, Moustafa M, Yasin S (2021) Efficiency boost of CZTS solar cells based on double-absorber architecture: device modeling and analysis. *Sol Energy* 225(9):44–52
- Arévalo P, Cano A, Benavides J, Jurado F (2021) Feasibility study of a renewable system (PV/HKT/GB) for hybrid tramway based on fuel cell and super capacitor. *IET Renewable Power Gen* 15(3):491–503
- Boldoo T, Lee M, Cho H (2022) Enhancing the solar energy conversion and harvesting characteristics of multiwalled carbon nanotubes-modified 1-hexyl-3-methyl-imidazolium cation ionic liquids. *Int J Energy Res* 46(7):8891–8907
- Dhimish M, Schofield N (2022) Single-switch boost–buck DC–DC converter for industrial fuel cell and photovoltaics applications. *Int J Hydrogen Energy* 47(2):1241–1255
- Falehi AD, Torkaman H (2021) Robust fractional-order super-twisting sliding mode control to accurately regulate lithium-battery/super-capacitor hybrid energy storage system. *Int J Energy Res* 45(13):18590–18612
- Ingrosso C, Valenzano V, Corricelli M, Testolin A, Curri ML (2021) PbS nanocrystals decorated reduced graphene oxide for nir responsive capacitive cathodes. *Carbon* 182(5):57–69
- Karunanithi K, Ramesh S, Raja SP, Sreedhar R, Kannan S, Ramudu V (2023) Investigations of standalone PV system with battery-supercapacitor hybrid energy storage system for household applications. *Int J Inf Technol* 15(1):279–287
- Maihulla AS, Yusuf I, Bala SI (2022) Reliability and performance analysis of a series–parallel system using Gumbel-Hougaard family copula. *J Comput Cogn Eng* 1(2):74–82
- Murthy LNS, Zhang B, Hsu JWP (2020) A device architecture study in fullerene-based organic photovoltaics. *J Phys Chem C* 124(24):12982–12989
- Nakhli MS, Shahbaz M, Ben Jebli M, Wang S (2022) Nexus between economic policy uncertainty, renewable & non-renewable energy and carbon emissions: contextual evidence in carbon neutrality dream of USA. *Renewable Energy* 185(1):75–85
- Rajulapati A, Mahalingam P (2022) High gain multi-input converter with inherent current sharing mechanism for photovoltaic applications. *Sol Energy* 233(1):118–133
- Ren G, Zhuang D, Zhao M, Wei Y, Li Y (2020) CZTSSe solar cell with an efficiency of 10.19% based on absorbers with homogeneous composition and structure using a novel two-step annealing process. *Sol Energy* 207(9):651–658

- Rezzak D, Boudjerda N (2020) Robust energy management strategy based on non-linear cascade control of fuel cells-super capacitors hybrid power system. *Int J Hydrogen Energy* 45(43):23254–23274
- Sajjad M, Javed MS, Imran M, Mao Z (2021) CuCo_2O_4 nanoparticles wrapped in a rGO aerogel composite as an anode for a fast and stable Li-ion capacitor with ultra-high specific energy. *New J Chem* 45(44):20751–20764
- Salameh T, Abdelkareem MA, Olabi AG, Sayed ET, Al-Chaderchi M, Rezk H (2021) Integrated standalone hybrid solar PV, fuel cell and diesel generator power system for battery or supercapacitor storage systems in Khorfakkan, United Arab Emirates. *Int J Hydrogen Energy* 46(8):6014–6027
- Sarker S, Islam MT, Rauf A, Jame HA, Ahmed S (2021) A SCAPS simulation investigation of non-toxic MgIn_2S_3 -on-Si tandem solar device utilizing monolithically integrated (2-T) and mechanically stacked (4-T) configurations. *Sol Energy* 225(9):471–485
- Uno M, Cheng D, Onodera S, Sasama Y (2023) Bidirectional buck-boost converter using cascaded energy storage modules based on cell voltage equalizers. *IEEE Trans Power Electron* 38(1):1249–1261
- Verkholyak T, Kuzmak A, Kornyshev AA, Kondrat S (2022) Less is more: can low quantum capacitance boost capacitive energy storage? *J Phys Chem Lett* 13(47):10976–10980
- Yassin AMM, Hassan MA, Elmesmary HM (2022) Key elements of green supply chain management drivers and barriers empirical study of solar energy companies in South Egypt. *Int J Energy Sect Manage* 16(3):564–584
- Ying C, Chen Y, Yang H, Mariotti D, Bo Z (2022) Regulation of electrode–electrolyte interactions for improved heat recovery of a thermo-induced electric double-layer capacitor. *Energy Fuels* 36(6):3304–3312

Publisher's Note

Springer Nature remains neutral with regard to jurisdictional claims in published maps and institutional affiliations.